International Journal of Pure and Applied Mathematics

Volume 30 No. 3 2006, 287-304

A BIDOMAIN MODEL OF HUMAN CARDIAC TISSUE INCORPORATING A CAPILLARY MICROSTRUCTURE

John C. Clements[1] §, B. Milan Horáček[2]

[1]Department of Mathematics and Statistics
School of Biomedical Engineering
Chase Building, Dalhousie University
Halifax, Nova Scotia, B3H 3J5, CANADA
e-mail: john.clements@dal.ca

[2]Department of Physiology and Biophysics and Department of Medicine
Tupper Building, Dalhousie University
Halifax, Nova Scotia, B3H 4H7, CANADA
e-mail: milan.horacek@dal.ca

Abstract: Experimental evidence has shown that during propagation of activation in mammalian cardiac tissue, fast action potential upstrokes ($\dot{V}_{max}$) and slower wave velocities are associated with transverse propagation while slow upstrokes and higher wave speeds are associated with longitudinal propagation. Standard bidomain models of cardiac dynamics cannot reproduce this behaviour nor do they incorporate the potentially important properties of the cardiac capillary network. In this study the standard continuous, anisotropic bidomain model for the propagation of electrical activation in the human myocardium H is extended to incorporate both a directionally dependent *bulk* membrane capacitance C_{blk} and a distributed parallel resistance-capacitance capillary network. Using a simple model for the cardiac membrane dynamics, numerical simulations are conducted to determine the propagation properties of the activation wavefronts for this modified formulation and to examine the extent to which the incorporation of this capillary microstructure affects the

Received: June 1, 2006

§Correspondence author

action potential profile.

AMS Subject Classification: 35K60, 92C05, 35Q80, 92C30
Key Words: mammalian cardiac tissue, anisotropic bidomain model, human myocardium, cardiac membrane dynamics, capillary microstructure

1. Introduction

Comprehensive heart models which simulate the propagation of realistic cardiac action potentials are important because the results can be compared with data from experiments on intact hearts [29, 4, 15], with clinical recordings obtained from the human heart *in situ* and with body surface potential map information [30, 13]. Such models have the potential to: (i) non-invasively locate and quantify arrhythmogenic substrate in cardiac patients, (ii) assess the effects of possible antiarrhythmic drug therapies and (iii) predict the consequences of pacing/cardioversion and other clinical interventions. Thus, it is important to have computationally tractable mathematical models which incorporate the relevant physiological structures and can reproduce those specific action potential properties which have been identified by experimental analysis – even if these models do not include detailed membrane dynamics at the microscopic level [16, 2, 3, 18]. In the past two decades, standard bidomain models have been constructed to simulate and study the propagation of excitation in representative slabs of cardiac tissue and, in some cases, whole heart geometries [8, 12, 16, 17, 19, 1, 6]. However, these models do not incorporate mechanisms to account for the fact that: (i) the rate of rise of the action potential upstroke ($\dot{V}$) is dependent on the direction of wave front propagation and (ii) the capillary network may exert a significant influence on the propagation properties of the transmembrane (V_m) and extracellular (ϕ_e) potentials.

Experimental evidence and modeling studies have shown [23, 24, 25, 9, 26, 27] that during propagation of activation in mammalian cardiac tissue, fast upstrokes ($\dot{V}_{max}$) and slower wave velocities are associated with transverse propagation while slow upstrokes and higher wave speeds are associated with longitudinal propagation. More specifically, it has been shown that $\dot{V}_{max}$ varies from 123 to 197 V/s during longitudinal propagation and from 140 to 240 V/s during transverse propagation [26]. It was also identified by Spach et al [25] that "the direction-dependent shape changes behave as though there is a directional difference in the 'effective' membrane capacitance". Indeed, in [25] the simulation results obtained for two one-dimensional cables closely resemble

typical anisotropic changes in experimentally measured upstrokes. Figure 1 in [25] illustrates this comparison using a specific membrane capacitance value of $C_m = 1.0$ (μF/cm^2) (giving $\dot{V}_{max} \cong 135$ V/s) for longitudinal propagation and a value of $C_m = 0.5$ (giving $\dot{V}_{max} \cong 240$ V/s) for transverse propagation. Standard bidomain models cannot reproduce this directionally dependent behaviour of the action potential profile. A second and perhaps more important consideration is the incorporation of a cardiac capillary network. In [26] Spach et al constructed a "2-domain" cellular network model of myocytes and capillaries separated by interstitial space. Part of their study included an examination of the time course of (the foot of) the action potential during propagation [26, 10]. They concluded that the passive capillary microstructure may induce a "feedback effect" which slows the initial rise of the action potential τ_{foot}. However, it was subsequently argued [20, 21] that the changes in the shape of the action potential foot which were observed experimentally may actually be due to the presence of a perfusing bath and not a consequence of the influence of the capillary microstructures. This is one of the issues which will be examined in this work.

Standard bidomain theory for cardiac tissue H assumes two interpenetrating anisotropic media – intracellular (i) and extracellular (e) – connected everywhere via the cell membrane [14]. Four local parameters $\sigma^{i,e}_{L,T}$ specify conductivities in the longitudinal (L) and transverse (T) directions with respect to cardiac muscle fibers. At the macroscopic level, propagation of electrical activation in H is defined by a coupled system of nonlinear elliptic-parabolic partial differential equations together with appropriate boundary conditions. Systems of ordinary differential equations model the cardiac membrane dynamics. In these models the specific membrane capacitance is assumed to be uniformly constant in all directions and is normally given the value $C_m = 1.0$ (μF/cm^2). Furthermore, there is no inclusion of terms to reflect the effects on the propagating action potential due to the presence of a passive capillary network. In Section 2 we extend the differential equations defining the macroscopic propagation properties of the bidomian to incorporate a directionally dependent *bulk* membrane capacitance C_{blk} and a distributed parallel resistance-capacitance capillary network. The model is first derived for a single uniform cylindrical fibre (cf. Figures 1(a)-1(c) and equations (5)-(6)) and then generalized to the equivalent formulation in R^3 defined by equations (8)-(9). Here we have attempted to include the essential components of the capillary microstructure described in [26], that is, the capacitive and resistive properties of the capillary wall.

We assume that the internal resistance of the capillary structures is small

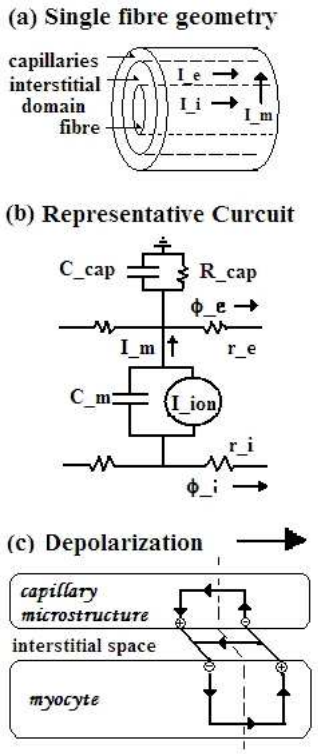

Figure 1: The *extended* bidomain model for a one-dimensional cylindrical fibre geometry with capillary microstructure

and can be neglected. This assumption appears reasonable since the conductivity of blood is large compared to that of the other extracardiac tissues [22]. A particular advantage of this modified formulation is that (8)-(9) is now a well-posed problem with a unique solution $\{V_m(\mathbf{x},t), \phi_e(\mathbf{x},t)\}$ for any choice of initial values $\{V_m(\mathbf{x},0), \phi_e(\mathbf{x},0)\}$. This is not true for the standard bidomain formulation. Indeed, in order to solve the standard formulation an artificial condition such as a point of grounded potential on the domain boundary is required. Here no such artificial condition is necessary. Furthermore, this modified formulation is considerably easier to solve using standard numerical techniques for reaction-diffusion systems. Using the same Fitz-Hugh Nagumo type membrane dynamics model employed in [16, 6], numerical simulations were conducted to determine the propagation properties of the activation wavefronts for this new formulation and to examine the extent to which this incorporation of capillary microstructure affects the foot of the action potential profile.

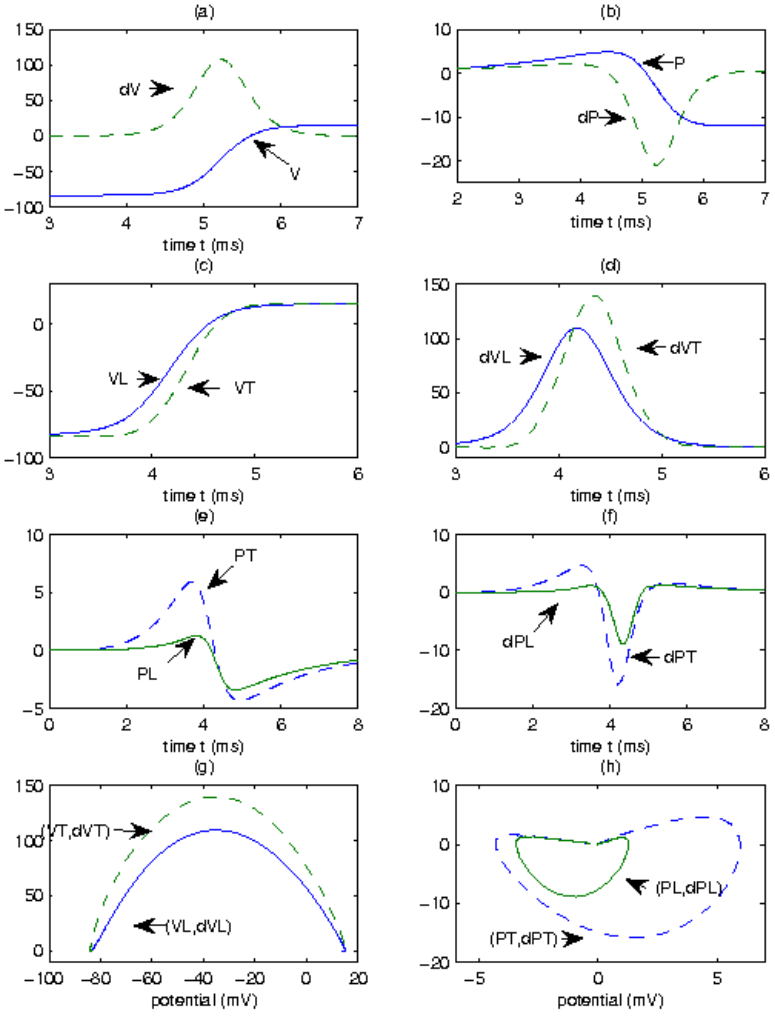

Figure 2: Comparison of V_m and ϕ_e dynamics for the *standard* ((a),(b)) and *extended* bidomain models ((c)-(h)). Potentials are in (mV), time is in (ms) and derivatives are in (mV/ms). (a) $V_m(t) = V$, $\dot{V}_m(t) = dV$; (b) $\phi_e(t) = P$, $\dot{\phi}_e(t) = dP$; (c) $V_{mL}(t) = VL$, $V_{mT}(t) = VT$; (d) $\dot{V}_{mL}(t) = dVL$, $\dot{V}_{mT}(t) = dVT$; (e) $\phi_{eL}(t) = PL$, $\phi_{eT}(t) = PT$; (f) $\dot{\phi}_{eL}(t) = dPL$, $\dot{\phi}_{eT}(t) = dPT$; (g) $(V_{mL}, \dot{V}_{mL})$=(VL, dVL); $(V_{mT}, \dot{V}_{mT})$ =(VT, dVT); (h) $(\phi_{eL}, \dot{\phi}_{eL}) = (PL, dPL)$; $(\phi_{eT}, \dot{\phi}_{eT}) = (PT, dPT)$.

2. The Extended Bidomain Model

We first derive a one-dimensional formulation of the extended bidomain model. Consider an arbitrary segment $[x_1, x_2]$ (cms) of a uniform cylindrical fibre of

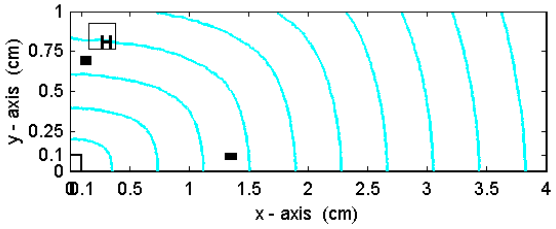

Figure 3: V_m isochrones of activation for the *extended* model displayed in H at 5 ms time intervals for 50 ms.

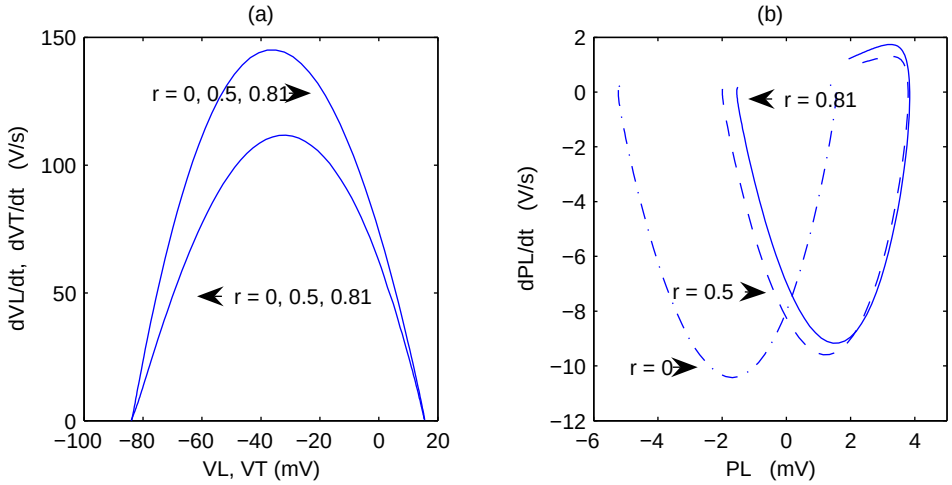

Figure 4: (a) $V_{mL}(t) = VL$ and $V_{mT}(t) = VT$ phase portraits for $r = \chi_{cap}/\chi_m = 0, .5, .81$; (b) $\phi_{eL}(t) = PL$ phase portraits for $r = 0, .5, .81$.

radius a (cm) (the intracellular region) lying within a cylindrical volume conductor of radius b (the extracellular or interstitial region) and surrounded by a region of capillary microstructures as in Figure 1(a). For the passive parallel resistance-capacitance capillary network lying between x_1 and x_2 [26, 10], let C_{cap} (μF/cm^2) be the specific capacitance, R_{cap} (kΩ cm^2) the specific resistance and I_c (μA/cm^2) the current per unit area of the capillary wall region as shown in Figure 1(b). If P_{cap} (cm) is the total perimeter of the capillary wall microstructures, then the total current per unit length across the capillary walls is $i_{cap} = P_{cap}I_{cap} = c_{cap}\frac{\partial \phi_e}{\partial t} + \frac{\phi_e}{r_{cap}}$, where $c_{cap} = P_{cap}C_{cap}$ (μF/cm) and $r_{cap} = R_{cap}/P_{cap}$ (kΩ cm). Let $I_i(x,t) = A_i\mathbf{i}_i(x,t)$ and $I_e(x,t) = A_e\mathbf{i}_e(x,t)$ (μA) denote the current flows in the positive axial direction in each region,

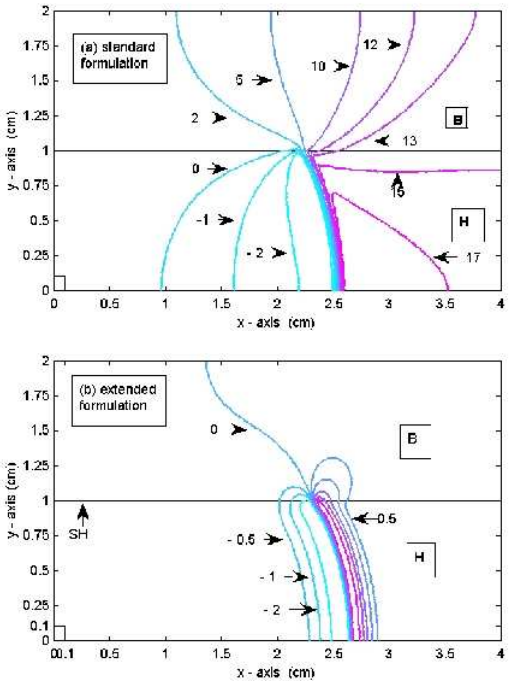

Figure 5: ϕ_e, ϕ_B dynamics for the $H \cup B$ geometry. (a) *standard* formulation: isopotential lines $\phi_e = \phi_B = -2, -10, 2, 5, 10, 12, 13, 15, 17$ mV at $t = 35$ ms; (b) *extended* formulation: isopotential lines $\phi_e = \phi_B = -2, -1, -0.5, 0, 0.5, 1, 2, 3, 4, 5$ mV at $t = 35$ ms.

where A_i and A_e (cm^2) are the respective cross-sectional areas and $\mathbf{i}_i(x,t)$ and $\mathbf{i}_e(x,t)$ (μA/cm^2) are the respective current densities. r_i and r_e (kΩ/cm) are the resistances per unit length of the intracellular and interstitial domains as in Figure 1(b). $\phi_i(x,t)$ and $\phi_e(x,t)$ (mV) denote the intracellular and interstitial potentials, respectively. Let i_{iapp} and i_{eapp} (μA/cm) be the currents per unit length applied to the intracellular and interstitial spaces, respectively and let i_m (μA/cm) denote the transmembrane current per unit length introduced along the line from the intracellular region to the interstitial region. From Figure 1(b), conservation of charge requires that the loss in current flow between x_1 and x_2 must equal the current required to charge each line between x_1 and x_2

plus the current "lost" due to the transmembrane and applied currents

$$\begin{aligned} I_e(x_1,t) - I_e(x_2,t) &= -\int_{x_1}^{x_2} \frac{\partial I_e}{\partial x} dx \\ &= \int_{x_1}^{x_2} (c_{cap}\frac{\partial \phi_e}{\partial t} + \frac{\phi_e}{r_{cap}})dx + \int_{x_1}^{x_2} (-i_m - i_{eapp})dx\,, \qquad (1) \\ I_i(x_1,t) - I_i(x_2,t) &= -\int_{x_1}^{x_2} \frac{\partial I_i}{\partial x} dx = \int_{x_1}^{x_2} (i_m - i_{iapp})dx. \end{aligned}$$

Since $[x_1, x_2]$ was arbitrary, this gives

$$i_m = \frac{\partial I_e}{\partial x} + c_{cap}\frac{\partial \Phi_e}{\partial t} + \frac{\phi_e}{r_{cap}} - i_{eapp} = -\frac{\partial I_i}{\partial x} + i_{iapp}\,, \qquad (2)$$

or

$$c_{cap}\frac{\partial \phi_e}{\partial t} + \frac{\partial (I_i + I_e)}{\partial x} + \frac{\phi_e}{r_{cap}} = i_{iapp} + i_{eapp}. \qquad (3)$$

For simplicity here we set $i_{app} = i_{iapp} = -i_{eapp}$. Ohm's Law requires that the total voltage loss from x_1 to x_2 must be the result of the total resistance loss along each segment or $-(1/r_e)\frac{\partial \phi_e}{\partial x} = I_e$, $-(1/r_i)\frac{\partial \phi_i}{\partial x} = I_i$. Thus (3) becomes

$$c_{cap}\frac{\partial \phi_e}{\partial t} - ((1/r_e)\frac{\partial^2 \phi_e}{\partial x^2} + (1/r_i)\frac{\partial^2 \Phi_i}{\partial x^2}) + \frac{\phi_e}{r_{cap}} = 0 \qquad (4)$$

which be written in terms of the transmembrane potential $V_m = \phi_i - \phi_e$ as

$$c_{cap}\frac{\partial \phi_e}{\partial t} - (1/r_i + 1/r_e)\frac{\partial^2 \phi_e}{\partial x^2} + \frac{\phi_e}{r_{cap}} = (1/r_i)\frac{\partial^2 V_m}{\partial x^2}. \qquad (5)$$

The intracellular and interstitial domains are coupled through a distributed cellular membrane as in Figure 1 (b). For the transmembrane current per unit area of membrane I_m (μA/cm^2), conservation of charge again requires that the current flow across the membrane must equal the current required to charge the membrane plus the total current I_{ion} (μA/cm^2) due to the flow of ions across the membrane. That is, $I_m = C_m\frac{\partial V_m}{\partial t} + I_{ion}$, where C_m is the specific membrane capacitance (μF/cm^2). Since $i_m = P_m I_m$, where $P_m = 2\pi a$ (cm) is the perimeter of a cross-section of fibre, it follows from (2) that

$$c_m\frac{\partial V_m}{\partial t} - \frac{\partial^2 (1/r_i)V_m}{\partial x^2} = i_{app} - i_{ion}(V_m) + \frac{\partial^2 (1/r_i)\phi_e}{\partial x^2}\,, \qquad (6)$$

where $c_m = P_m C_m$ and $i_{ion}(V_m) = P_m I_{ion}(V_m)$. Equations (5) and (6) form the basis for the one-dimensional bidomain model incorporating capillary capacitance. Since we are concerned here with one-dimensional propagation, there can be no directional dependence of the membrane capacitance c_m or of the membrane surface area per unit volume.

For the equivalent anisotropic bidomain model in R^3 [6], the intracellular

Symbol	Parameter Definition	Value(s)	Units
C_L	longitudinal bulk membrane capacitance	1.0	μF/cm^2
C_T	transverse bulk membrane capacitance	0.7	μF/cm^2
χ_m	membrane suface area per unit volume	1000	cm^{-1}
σ_L^i	intracellular longitudinal conductivity	1.7	mS/cm
σ_T^i	intracellular transverse conductivity	0.19	mS/cm
σ_L^e	interstitial longitudinal conductivity	6.2	mS/cm
σ_T^e	interstitial transverse conductivity	2.4	mS/cm
σ_B	conductivity of extracardiac tissue region	2.0	mS/cm
C_{cap}	specific capacitance of capillary wall	1.0	μF/cm^2
R_{cap}	specific resistance of capillary wall	1.0	kΩ cm^2
χ_{cap}	capillary wall surface area per unit volume	$0-830$	cm^{-1}
r	ratio of surface areas χ_{cap}/χ_m	$0-.83$	

Table 1: Parameter values for extended bidomain model in R^3

and extracellular anisotropic conductivity properties of the myocardium H are specified by global coordinate tensors $\mathbf{D}_i$ and $\mathbf{D}_e$

$$\mathbf{D}_i = \sigma_T^i \mathbf{I} + (\sigma_L^i - \sigma_T^i)\mathbf{a}_L(\mathbf{x})\mathbf{a}_L'(\mathbf{x}), \qquad \mathbf{D}_e = \sigma_T^e \mathbf{I} + (\sigma_L^e - \sigma_T^e)\mathbf{a}_L(\mathbf{x})\mathbf{a}_L'(\mathbf{x}),$$

where $\mathbf{I}$ is the identity matrix, $\mathbf{a}_L(\mathbf{x})$ is the unit vector corresponding to the longitudinal fibre direction at each point $\mathbf{x}$ in the myocardium H, $\mathbf{a}_L'$ denotes the transpose of $\mathbf{a}_L$ and the four parameters $\sigma_{L,T}^{i,e}$ (mS/cm) specify local conductivities in the longitudinal (L) and transverse (T) directions with respect to the cardiac muscle fibers (see Table 1). The directional dependence of the "bulk" membrane capacitance due to the cell membrane, gap junctions and other microstructures [25] is incorporated into the model by defining C_{blk} (μF/cm^2) as

$$C_{blk} = C_T + (C_L - C_T)\frac{|\nabla V_m \bullet \mathbf{a}_L|}{\|\nabla V_m\|}, \tag{7}$$

where C_T and C_L are the "bulk" membrane capacitances in the transverse and longitudinal directions, respectively and $C_{blk} \geq \min\{C_L, C_T\} > 0$. From (7) it is seen that C_{blk} depends on the angle which the propagating wave front makes with the longitudinal fibre direction $\mathbf{a}_L(\mathbf{x})$ and varies continuously from C_L when the wave front is parallel to $\mathbf{a}_L(\mathbf{x})$ to C_T when the propagation is transverse to the local fibre direction. The simple form of (7) does not add significantly to the computational load required to solve the bidomain equations.

The membrane surface area per unit volume χ_m (cm^{-1}) sets the length scales $\sqrt{\frac{\sigma_L^i \sigma_L^e}{(\sigma_L^i+\sigma_L^e)\chi_m C_m}}$ and $\sqrt{\frac{\sigma_T^i \sigma_T^e}{(\sigma_T^i+\sigma_T^e)\chi_m C_m}}$ in the longitudinal and transverse directions and determines the wave speeds in these respective directions. In terms of the transmembrane V_m and extracellular ϕ_e potentials, the extended bidomain model for the propagation of electrical activation in the three-dimensional anisotropic cardiac tissue H is defined in terms of current per unit volume by the reaction-diffusion equations

$$\begin{aligned} c_{cap}\frac{\partial \phi_e}{\partial t} - \nabla \cdot (\mathbf{D}_i \nabla (V_m + \phi_e) + \mathbf{D}_e \nabla \phi_e) + \frac{\phi_e}{r_{cap}} = 0\,, \\ c_{blk}\frac{\partial V_m}{\partial t} - \nabla \cdot \mathbf{D}_i \nabla (V_m + \phi_e) = i_{app} - i_{ion}(V_m)\,, \end{aligned} \tag{8}$$

and the homogeneous boundary conditions [6]

$$\mathbf{n} \cdot \mathbf{D}_e \nabla \phi_e = 0, \quad \mathbf{n} \cdot \mathbf{D}_i \nabla (v_m + \phi_e) = 0 \text{ on } S_H\,, \tag{9}$$

where χ_{cap} (cm^{-1}) is the (constant) capillary wall surface area per unit volume, i_{app} ($\mu\mathrm{A/cm}^3$) is the applied current per unit volume initiating the activation, $i_{ion}(V_m, u) = \chi_m I_{ion}(V_m, u)$ ($\mu\mathrm{A/cm}^3$) is the total ionic current across the cell membrane per unit volume, $c_{blk} = \chi_m C_{blk}$ ($\mu\mathrm{F/cm}^3$), $c_{cap} = \chi_{cap} C_{cap}$ ($\mu\mathrm{F/cm}^3$) and $r_{cap} = R_{cap}/\chi_{cap}$ ($\mathrm{k}\Omega\ \mathrm{cm}^3$). The membrane dynamics $i_{ion}(V_m, u)$ were modeled using the same FutzHugh-Nagumo model employed in [16]

$$\begin{aligned} I_{ion} &= d_1 (V_m - V_{rest})(1 - \frac{(V_m - V_{rest})}{5.0})(1 - \frac{(V_m - V_{rest})}{100.0}) \\ &\quad + 0.02(V_m - V_{rest})u\,, \\ \frac{du}{dt} &= d_2((V_m - V_{rest}) - 0.005u); \quad u(0) = 0\,, \end{aligned} \tag{10}$$

where $d_1 = 0.5$, $d_2 = 0.015$ and u is the recovery variable. This model produces a reasonable morphology for an action potential of 100 ms duration. Unlike the more comprehensive models [2, 3, 18], it cannot produce response refractoriness. The capillary wall time constant is $\tau_{cap} = C_{cap}/R_{cap}$ (ms). It is independent of the geometry of the wall structure and is a measure of the time required for a transient response to current input I_{cap} to attain a substantial fraction of its steady-state. This is reflected in the translation of the current maxima (+) and minima (-) illustrated in Figure 1(c) and described in [26, 5].

3. Numerical Simulations

3.1. An Isolated Bidomain Region H

The myocardial tissue geometry H is represented here by a two-dimensional, uniformly anisotropic 1 cm $\times$ 4 cm sheet (cf. Figure 3). This could be viewed as a thin horizontal slice of tissue from the lateral wall of the ventricles. This slice would be taken perpendicular to the vertical axis of the heart with the x-axis $0 \le x \le 4$ representing the endocardial surface and the boundary $y = 1$, $0 \le x \le 4$ representing the epicardial surface. The longitudinal fibre direction L is assumed to be parallel to the x-axis at each point and the transverse direction T is parallel to the y-axis. The "bulk" membrane capacitances in the transverse and longitudinal directions are taken to be $C_T = 0.7$ and $C_L = 1.0$. As in [26], $C_L = 1.0$ agrees with C_m for the standard bidomain formulation. The membrane surface area per unit volume parameter $\chi_m = 1000$ cm^{-1} yields longitudinal and transverse wave speeds in the range of $\theta_L = 0.76$ m/s and $\theta_T = 0.38$ m/s, respectively. The conductivity values $\sigma^{i,e}_{L,T}$ in Table 1 are taken from [7] and represent measured electrical properties for trabecular bundles from the right ventricle of calf hearts. In accordance with the remaining values employed in [26], $C_{cap} = 1.0$ μF/cm^3 while χ_{cap} ranges in value from 0 to $0.83\chi_m = 830$ cm^{-1}. The range for χ_{cap} corresponds to the experimental estimates for capillary density. These estimates are that the ratio $r = \chi_{cap}/\chi_m$ of the area of capillary wall to myocyte membrane area is 0 for neonatal myocardial tissue and 0.83 for adult ventricular muscle. The value for R_{cap} was chosen to be 1 kΩ which is roughly representative of the values considered in [26]. Indeed, repeated trials with R_{cap} ranging over $0 \to 8$ kΩ produced only minor changes in the results obtained. For this geometry, the extended model formulation (8)-(9) in conservation form becomes

$$d_a \frac{\partial \mathbf{u}}{\partial t} + \nabla \cdot \mathbf{\Gamma} = \mathbf{F}, \quad \mathbf{u}(0) = \mathbf{u}_o \text{ in } H, \quad -\mathbf{n} \cdot \mathbf{\Gamma} = \mathbf{0} \text{ on } S_H\,, \tag{11}$$

where

$$\nabla \cdot \mathbf{\Gamma} = \begin{pmatrix} -\sigma^i_L(\frac{\partial^2 V_m}{\partial x^2} + \frac{\partial^2 \phi_e}{\partial x^2}) - \sigma^e_L \frac{\partial^2 \phi_e}{\partial x^2} - \sigma^i_T(\frac{\partial^2 V_m}{\partial y^2} + \frac{\partial^2 \phi_e}{\partial y^2}) - \sigma^e_T \frac{\partial^2 \phi_e}{\partial y^2} \\ -\sigma^i_L(\frac{\partial^2 V_m}{\partial x^2} + \frac{\partial^2 \phi_e}{\partial x^2}) - \sigma^i_T(\frac{\partial^2 V_m}{\partial y^2} + \frac{\partial^2 \phi_e}{\partial y^2}) \end{pmatrix},$$

$$\mathbf{u} = \begin{pmatrix} \phi_e \\ V_m \end{pmatrix}, \quad d_a = \begin{pmatrix} c_{cap} & 0 \\ 0 & c_{blk} \end{pmatrix}, \quad \mathbf{F} = \begin{pmatrix} -\frac{\phi_e}{r_{cap}} \\ i_{app} - i_{ion}(V_m) \end{pmatrix},$$

$$\mathbf{u}_o = \begin{pmatrix} 0 \\ V_{rest} \end{pmatrix}$$

and

$$-\mathbf{n}\cdot\mathbf{\Gamma} = \begin{pmatrix} n_x(\sigma_L^i(\frac{\partial V_m}{\partial x}+\frac{\partial \phi_e}{\partial x})+\sigma_L^e\frac{\partial \phi_e}{\partial x})+n_y(\sigma_T^i(\frac{\partial V_m}{\partial y}+\frac{\partial \phi_e}{\partial y})+\sigma_T^e\frac{\partial \phi_e}{\partial y}) \\ n_x\sigma_L^i(\frac{\partial V_m}{\partial x}+\frac{\partial \phi_e}{\partial x})+n_y\sigma_T^i(\frac{\partial V_m}{\partial y}+\frac{\partial \phi_e}{\partial y}) \end{pmatrix}.$$

Since activation normally occurs from the endocardium to the epicardium, the activation sequence was initiated by an applied current stimulus $I_{app} = 35\cos(\pi x/.2)\cos(pi * y/.2)$ μA/cm^2 over a small region [0.1,0]x[0,0.1] at (0,0) for a 0.2-ms duration. All simulations were performed using the finite element software *FEMLAB/MATLAB* [11] with a maximum relative error tolerance of 1.0×10^{-5}.

Figure 2 provides a comparison of the time dynamics of V_m and ϕ_e for the *standard* and *extended* bidomain model formulations in H. For these comparisons, χ_{cap} is set to 830 cm^{-1} (adult mammalian heart) in the extended model. To provide a basis for comparison, Figures 2(a), (b) display the plots of V_m, $\dot{V}_m = \frac{dV_m}{dt}$, ϕ_e, and $\dot{\phi}_e = \frac{d\phi_e}{dt}$ at the point $(1.0, 0.5)$ in H for the *standard* bidomain model. Although V_m is the same smooth curve from -84 mV to 16 mV at every point of H (Figure 2(a)) and the general shape of the $\phi_e(t) = P$ curve is that given in Figure 2(b), the range of values for $\phi_e(t)$ were found to vary somewhat depending on which point in H was selected. For the point $(x, y) = (1, 0.5)$ in H, $\phi_e(t)$ varied from 5.0 mV to -12.6 mV as indicated in Figure 2(b). However, just behind the wave front the range for ϕ_e changes to $17 \rightarrow -2$ mV. Note that $\max\{\dot{V}_m\} = 110$ V/s during both longitudinal and transverse propagation for the standard formulation. The longitudinal (L) and transverse (T) potentials for the *extended* model are the computed values of V_m and ϕ_e at the points $(1.4, 0.01)$ (longitudinal) and $(0.01, 0.7)$ (transverse) in H. These points are indicated by solid rectangles in Figure 3. Figures 2(c),(d) compare V_{mL}, V_{mT} and $\dot{V}_{mL}$, $\dot{V}_{mT}$ for the extended model formulation. Again, both V_{mL} and V_{mT} range from -84 mV to 16 mV (Figure 2(c)) but now with different rates of upstroke; $\max\{\dot{V}_{mL}\} = 110$ V/s while $\max\{\dot{V}_{mT}\} = 140$ V/s (Figure 2(d)). Similarly, Figures 2(e),(f) compare ϕ_{eL}, ϕ_{eT} and $\dot{\phi}_{eL}$, $\dot{\phi}_{eT}$ for the extended model. ϕ_{eL} ranges from 1.7 mV to -3.6 mV, ϕ_{eT} ranges from 7.0 mV to -4.5 mV with $\max|\{\dot{\phi}_{eL}|\} = 9$ V/s and $\max\{|\dot{\phi}_{eT}|\} = 16$ V/s. The directional *bulk* membrane capacitance produces the required differential in the rate of action potential upstroke as shown in Figure 2(d) and, as expected, also generates a directional difference in the shape of the extracellular potential curves ϕ_{eL} and ϕ_{eT} as can be seen in Figures 2(e),(f). The capillary network terms appear to produce reduced ranges (particularly for ϕ_{eL}) and much more

regular morphologies for the ϕ_{eL} and ϕ_{eT} curves when compared with the behaviour of ϕ_e in the standard model. Figures 2(e),(f) display the phase portraits $(V_{mL}, \dot{V}_{mL})$, $(V_{mT}, \dot{V}_{mT})$, $(\phi_{eL}, \dot{\phi}_{eL})$ and $(\phi_{eT}, \dot{\phi}_{eT})$ for the extended model.

Figure 3 displays the isochrones of activation at 5 ms time intervals for 50 ms for the *extended* model with $\chi_{cap} = 830$. The wave front was determined at each time step by identifying those mesh points in H, where the transmembrane potential V_m attains the value 10 mV (from a rest value of -84 mV). Figure 4(a) displays the *extended* model phase portraits $(V_{mL}(t), \dot{V}_{mL}(t))$ and $(V_{mT}(t), \dot{V}_{mT}(t))$ for the ratio of capillary wall to membrane surface area per unit volume parameter $r = \chi_{cap}/\chi_m = 0, .5, .81$. $r = \chi_{cap}/\chi_m$ is a measure of the relative density of the capillary network structure and the range of values examined here corresponds to that chosen in [26]. What is immediately evident from Figure 4(a) is that the capillary microstructures appear to have no discernable effect on the foot of V_m for the relative densities $r = 0 \rightarrow .81$. Figure 4(b) displays the *extended* model phase portraits $(\phi_{eL}, \dot{\phi}_{eL})$ for the longitudinal interstitial potential ϕ_{eL} with $r = \chi_{cap}/\chi_m = 0, .5, .81$. The phase portraits for ϕ_{eT} are not plotted since they are virtually identical to those obtained for ϕ_{eL} with only a modest phase shift being the evident difference. As can be seen in Figure 4(b), the capillary microstructures have a fairly pronounced effect on the phase portraits for the interstitial potentials, but again, not on the foot of these potentials. The full extent of the effect of the capillary network is clearly illustrated in Figures 5(a),(b) in the next example.

3.2. A Bidomain Region Adjoined by Extracardiac Tissue, $H \cup B$

Here $H \cup B$ consists of a two-dimensional, uniformly anisotropic 1 cm $\times$ 4 cm sheet as above which is surmounted by a 1 cm $\times$ 4 cm homogeneous region B of conductivity $\sigma_B = 2.0$ mS/cm representing the extracardiac regions (cf. Figure 5). Let S_H and S_B denote the boundaries of H and B except for the common boundary line between the two domains $y = 1, 0 \leq x \leq 4$ (the epicardial surface). The line $y = 2, 0 \leq x \leq 4$ represents the torso surface and ϕ_B is the (quasi-static) potential at each point of B. Again, the longitudinal fibre direction L is taken to be parallel to the x-axis at each point and the transverse direction T is parallel to the y-axis. Homogeneous Neumann conditions are imposed on all vertical and horizontal boundaries except the common boundary at $y = 1$, where the condition of continuity of current flow is imposed. The

extended bidomain model for $H \cup B$ is then given by

$$\begin{aligned} d_a \frac{\partial \mathbf{u}}{\partial t} + \nabla \cdot \mathbf{\Gamma} = \mathbf{F}, \quad \mathbf{u}(0) = \mathbf{u}_o \text{ in } H, \quad -\mathbf{n} \cdot \mathbf{\Gamma} = \mathbf{G} \text{ on } S_H, \\ \nabla \cdot \mathbf{\Phi} = 0 \text{ in } B; \quad -\mathbf{n} \cdot \mathbf{\Phi} = 0 \text{ on } S_B, \quad \phi_e = \phi_B \text{ on } y = 1, \end{aligned} \tag{12}$$

where $\mathbf{\Phi} = \begin{pmatrix} -\sigma_B \frac{\partial \phi_B}{\partial x} \\ -\sigma_B \frac{\partial \phi_B}{\partial y} \end{pmatrix}$ and $\mathbf{G} = \mathbf{0}$ except for $y = 1$, when $\mathbf{n} = (0, 1)$ and

$$-\mathbf{n} \cdot \mathbf{\Gamma} = \begin{pmatrix} \sigma_T^i (\frac{\partial V_m}{\partial y} + \frac{\partial \phi_e}{\partial y}) + \sigma_T^e \frac{\partial \phi_e}{\partial y}) \\ \sigma_T^i (\frac{\partial V_m}{\partial y} + \frac{\partial \phi_e}{\partial y}) \end{pmatrix} = \begin{pmatrix} \sigma_B \frac{\partial \phi_B}{\partial y} \\ 0 \end{pmatrix}. \tag{13}$$

The isopotential lines for ϕ_e and ϕ_B at time $t = 35$ ms are displayed in Figure 5(a) for the *standard* formulation with bulk membrane capacitance included but without any capillary microstructure terms and in Figure 5(b) for the *extended* formulation with $C_{cap} = 830$ and $R_{cap} = 1.0$. In Figure 5(a) the contours correspond to $\phi_e = \phi_B = -2, -1, 0, 2, 5, 10, 12, 13, 15, 17$ mV at $t = 35$ ms. In Figure 5(b) the contours correspond to $\phi_e = \phi_B = -2, -1, -0.5, 0, 0.5, 1, 2, 3, 4, 5$ mV at $t = 35$ ms. What it clear from a comparison of these contour lines is that introduction of a capillary microstructure has a fairly significant effect on the potential distributions near the wave front for ϕ_e and on the potential distribution ϕ_B in B at each instant of time.

4. Discussion

While there is general agreement that at the cellular level the propagation of activation in cardiac tissue is essentially a discontinuous process [28], there is still value in developing a continuous model which is capable of simulating at the macroscopic level the action potential profiles observed experimentally. This is particularly true with regard to the study of the properties of the wavefronts of activation. In this work we have extended the standard continuous, anisotropic bidomain model for cardiac tissue to incorporate (i) a directionally dependent *bulk* membrane capacitance C_{blk} and (ii) a resistance-capacitance capillary network, $\{C_{cap}, R_{cap}\}$. We have shown (cf. Figures 2(c), (d)) that introduction of the longitudinal and transverse bulk membrane capacitances CL and CT can reproduce experimentally measured rates of action potential upstroke in the respective directions. Our simplified version of the capillary network was based on work by Spach et al in [26]. We studied the effect of this simple microstructure on the propagation properties of the transmembrane and extracellular potentials and, in particular, on the foot of the action potential profile. For the range of capillary densities considered in [26], our simplified

capillary model appeared to generate no apparent influence on the foot of the longitudinal or transverse transmembrane potential profiles (cf. Figure 4(a)) nor did it affect the wavefront propagation properties of the transmembrane potential V_m. This appears to support the analysis found in [20, 21]. However, as was pointed out in [16], "no continuous or discrete model has completely accounted for both changes in $\dot{V}_{max}$ and τ_{foot} seen experimentally, suggesting that all the loading effects have not been included". In spite of this finding, the incorporation of a cardiac capillary network remains an important addition to the standard bidomain model formulations. Perhaps most interesting is the effect which our simple microstructure has on the spatial and time-course distributions of the extracellular and extracardiac potentials. This can be seen in Figures 2(c)-(h), Figure 4(b) and Figures 5(a), (b). The capillary structure generates a reduced range and more regular morphology for the extracellular potentials ϕ_e in H and a less dispersive pattern of extracardiac potential distributions ϕ_B in B. This suggests that the primary effect of the capillary network is to modify the phase portait behaviour of the extracellular potentials in H and the potential distributions in the extracardiac region B. This effect could be an important consideration when matching simulated and actual body surface potential map data using a bidomain model. Finally, the important advantages of the extended formulation is that: (i) it incorporates a relevant physiological structure, (ii) it results in a well-posed mathematical problem which does not require artificial conditions to ensure uniqueness and (iii) it lends itself to simpler more effective numerical solution techniques. Indeed, the capillary network terms stabilize the problem to such an extend that even very fast explicit solvers can be used with some accuracy.

Acknowledgments

This work was supported in part by research grants from the Natural Sciences and Engineering Council of Canada (NSERC), the Canadian Institutes of Health Research (CIHR) and the Heart and Stroke Foundation of Nova Scotia.

References

[1] O. Berenfeld, J. Jalife, Purkinje-muscle reentry as a mechanism of polymorphic ventricular arrhythmias in a 3-dimensional model of the ventricles, *Circ. Res.*, **82** (1998), 1063-1077.

[2] O. Bernus, R. Wilders, C.W. Zemlin, H. Verschelde, A.V. Panfilov, A

computationally efficient electrophysiological model of human ventricular cells, *Am. J. Physiol. Heart Circ. Physiol.*, **282** (2002), H2296-H2308.

[3] O. Bernus, H. Verschelde, A.V. Panfilov, Modified ionic models of cardiac tissue for efficient large scale computations, *Phys. Med. Biol.*, **47** (2002), 1947-1959.

[4] P.S. Chen, P.D. Wolf, S. Melnick, N.D. Danieley, W.M. Smith, R.E. Ideker, Comparison of activation during ventricular fibrillation and following unsuccessful defibrillation shocks in open-chest dogs, *Circ. Res.*, **66** (1990), 1544-1560.

[5] J.W. Clark, R. Plonsey, A mathematical study of nerve fibre interaction, *Biophys. J.*, **10** (1970), 937-957.

[6] John C. Clements, Juuka Nenonen, P.K.J. Li, B Milan Horáček, Activation dynamics in anisotropic cardiac tissue via de-coupling, *Ann. Biomed. Eng.*, **32**, No. 7 (2004), 984-990.

[7] L. Clerc, Directional differences of impulse spread in trabecular muscle from mammalian heart, *J. Physiol., Lond.*, **255** (1976), 335-346.

[8] P. Colli Franzone, L. Guerri, B. Taccardi, Potential distributions generated by point stimulation in a myocardial volume: Simulation studies in a model of anisotropic ventricular muscle, *J. Cardiovasc Electrophysiol*, **4** (1993), 438-458.

[9] C. Delgado, B. Steinhaus, M. Delmar, D.R. Chialvo, J. Jalife, Directional differences in excitability and margin of safety for propagation in sheep ventrical muscle, *Circ. Res.*, **67** (1990), 97-10.

[10] Vladimir G. Fast, André G. Kléber, Microscopic conduction in cultures strands of neonatal rat heart cells measured with voltage-sensitive dyes, *Circ. Res.*, **73** (1993), 914-925.

[11] *Femlab Reference MannualVersion 2.3*, Comsol AB, Sweden (2001).

[12] G. Fischer, B. Tilg, R. Modre, G.J.M. Huiskamp, J. Fetzer, W. Rucker, P. Wach, A bidomain model based BEM-FEM coupling formulation for anisotropic cardiac tissue, *Ann. Biomed. Eng.*, **11** (2000), 1229-1243.

[13] John R. Fitz-Clarke, *Spatiotemporal Dynamics of Ventricular Fibrillation in a Three-Dimensional Anisotropic Heart Model*, Ph.D. Thesis Dalhousie University (2003).

[14] D.B. Geselowitz, W.T. Miller, III, A bidomain model for anisotropic cardiac muscle, *Ann. Biomed. Eng.*, **28** (1983), 191-206.

[15] L.S. Green, B. Taccardi, P.R. Ershler, RL Lux, Epicardial potential mapping: Effects of conducting media on isopotential and isochrone distributions, *Circulation*, **84** (1991), 2513-2521.

[16] C.S. Henriquez, A.L. Muzikant, C.K. Smoak, Anisotropy, fiber curvature, and bath loading effects on activation in thin and thick cardiac tissue preparations: Simulations in a three-dimensional bidomain model, *J. Cardiovasc Electrophysiol*, **7** (1996), 424-444.

[17] G.J. Huiskamp, Simulation of depolarization in a membrane-equations-based model of the anisotropic ventrical, *IEEE Trans. Biomed. Eng.*, **45** (1998), 847-855.

[18] C-H Luo, Y Rudy, A model of the ventricular cardiac action potential: Depolarization, repolarization and their interaction, *Circ. Res.*, **68** (1991), 1501-1526.

[19] A.V. Panfilov, A.V. Holden, Editors, *Computational Biology of the Heart*, Wiley, New York (1997).

[20] Bradley J. Roth, Influence of a perfusing bath on the foot of the cardiac action potential, *Circ. Res.*, **86** (2000), e19-e22.

[21] Bradley J. Roth, Effect of a perfusing bath on the rate of rise of an action potential propagating through a slab of cardiac tissue, *Ann. Biomed. Eng.*, **24** (1996), 639-646.

[22] Stanley Rush, J.A. Abildskov, Richard McFee, Resistivity of body tissues at low frequencies, *Circulation Research*, **12** (1963), 40-50.

[23] M.S. Spach, W.T. Miller III, D.B. Geselowitz, R.C. Barr, J.M. Kootsey, E.A. Johnson, The discontinuous nature of propagation in normal canine cardiac muscle: Evidence for recurrent discontinuities of intracellular resitance that affect the membrane currents, *Circ. Res.*, **848** (1981), 39-54.

[24] M. S. Spach, W.T. Miller III, P.C. Dobler, J.M. Kootsey, J.R. Sommer, C.E. Mosher Jr., The functional role of structural complexities in the propagation of depolarization in the atrium of the dog. Cardiac conduction disturbances due to discontinuiuties of effective axial resistivity, *Circ. Res.*, **50**, No. 2 (1982), 175-191.

[25] Madison S. Spach, Paul C. Dolber, J. Francis Heidlage, J. Mailen Kootsey, Edward A. Johnson, Propagating depolarization in anisotropic human and canine cardiac muscle: apparent directional differences in membrane capacitance, *Circ. Res.*, **60** (1987), 206-219.

[26] Madison S. Spach, J. Francis Heidlage, Paul C. Dolber, Roger C. Barr, Extracellular discontinuities in cardiac muscle: evidence for capillary effects on the action potential foot, *Circ. Res.*, 83 (1998), 1144-1164.

[27] Madison S. Spach, Roger C. Barr, Effects of cardiac microstructure on propagating electrical waveforms, *Circ. Res.*, **86** (2000), e23-e28.

[28] Madison S. Spach, Transition from a continuous to discontinuous understanding of cardiac conduction, *Circ. Res.*, **92** (2003), 125.

[29] B. Taccardi, E. Macchi, R.L. Lux, P.E. Ershler, S. Spaggiari, S. Baruffi, and Y. Vyhmeister, Effect of myocardial fiber direction on epicardial potentials, *Circulation*, **90** (1994), 3076-3090.

[30] Lawrence M. Title, MD, Sian E. Iles, MD, Martin J. Gardner, MD, Cindy J. Penney, PhD, John C. Clements, PhD, B. Milan Horacek, PhD, Quantitative assessment of myocardial ischemia by electrocardiographic and scintigraphic imaging, *Journal of Electrocardiology*, **36**, Supplement (2003), 17-25.